1D+ model for overbank flows with a transition bed friction - emergent rigid vegetation drag

Sébastien Proust, J.B. Faure, V. Dupuis, Céline Berni, André Paquier

Author-produced version , River Flow 2016, Saint Louis, USA, 11-15 July 2016

1D+ model for overbank flows with a transition bed friction – emergent rigid vegetation drag

S. Proust, J.B. Faure, V. Dupuis, C. Berni, A. Paquier
Irstea-Lyon, Hydrology-Hydraulics research unit, Villeurbanne, France

ABSTRACT: This paper investigates the 1-D+ modelling of overbank flows in case where floodplains (FP) feature a streamwise roughness transition from bed-roughness to emergent rigid vegetation, or vice versa (representing *e.g.* a change from highly submerged dense meadows to emergent trees areas). The simulations are compared with experimental data collected in a compound channel flume. The meadow is physically modelled by artificial plastic grass and the trees by rigid stems. The upstream discharge distribution between the main channel (MC) and the FP is varied in order to alter the lateral mean flow between MC and FP. To account for the upstream discharge distribution, the 1D+ model developed by Proust *et al.* (2009), the Independent Subsections Method (ISM), is used. The volume drag force exerted by the stems is modelled by a formula established by Nepf (1999). The ability of ISM to predict flow depth, mean flow in the FP, and the depth-averaged Reynolds-stress at the junction MC/FP is assessed.

1 INTRODUCTION

When dealing with 1D modelling of non-uniform overbank flows, the backwater surface profile is commonly solved on the total compound cross-section, composed of a main channel (MC) and one or two floodplains (FP). This approach was found to be not suitable when an accurate prediction of both water level and discharge distribution between MC and FP is required (Proust *et al.* 2009). These authors also showed that this goal can be achieved by solving the surface profile in each sub-section (1D+ approach), using the so-called Independent Subsections Method (ISM). The ISM was validated against experimental data for both prismatic and non-prismatic geometries. For the 46 flow cases, the ISM predicted flow depth and mean velocity in the FP with a maximum relative error of 8% and 19%, respectively, which is far less than the classical 1D approaches (Proust *et al.* 2009). It is important to note that all the investigated flow configurations featured smooth FP.

The ISM was then tested against experimental data in skewed compound channels with smooth or rough FP by Jacqmin & Wyseur (2011). The relative errors on FP discharge and flow depth were found to be very small with smooth FP. However, preliminary results showed that they are likely to increase with bed-roughened FP.

The aim of the present study is to go further in the assessment of the ISM in the presence of bed-roughness over the FP, but also of emergent macro-roughness elements, as those physically modelled by Pasche & Rouve (1985) or Wormleaton & Merett (1990) under uniform flow conditions.

Additionally, the ability of the ISM to predict the depth-averaged Reynolds-stress at the junction MC/FP will also be assessed, which was not carried out by Proust *et al.* (2009) and Jacqmin & Wyseur (2011).

The ISM is used here to simulate non-uniform overbank flows in case where the FP feature a streamwise transition from bed-roughness to emergent macro-roughness as in the case of a change in land occupation from highly submerged dense meadows to emergent trees areas, or vice versa. These flows were physically modelled in a wide compound channel flume located in the Hydraulics and Hydromorphology Laboratory of Irstea Lyon-Villeurbanne (HHLab), France. The detailed experimental results are presented and analyzed in Dupuis (2016).

2 LABORATORY EXPERIMENTS

2.1 *The compound channel flume*

The experiments were performed in a 18 m long and 3 m wide glassed-wall compound channel flume (Fig. 1), which is located at Irstea, Lyon, France.

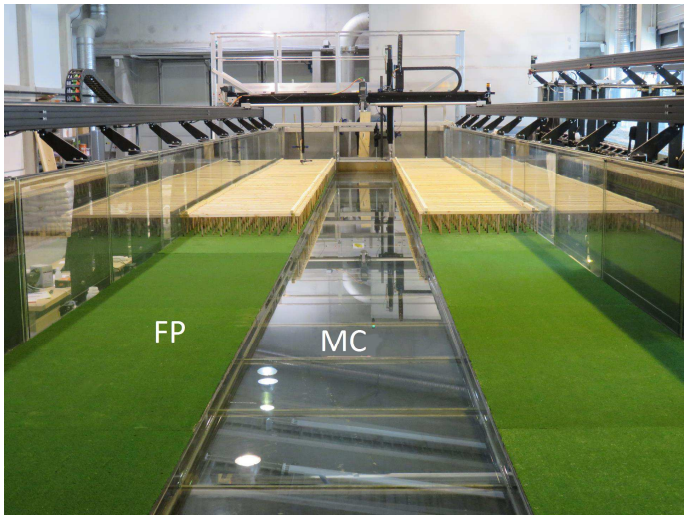

Figure 1. Picture from downstream of the glassed-wall compound channel flume (18m × 3m) located in the Hydraulics and Hydromorphology Laboratory of Irstea Lyon-Villeurbanne (HHLab). Transition "Stems / Meadow" over the floodplain (FP). The main channel is denoted MC.

The longitudinal bottom slope, S_0, is of 1.05/1000, the compound cross-section consists in a rectangular MC and two lateral FP, with sub-section widths $B_r = B_l = B_m = 1$ m where the subscripts l, r, and m refer to the left FP, right FP and MC, respectively. The dense meadow over the FP is modelled with artificial plastic grass, whose blades are 5 mm high. The bank full stage in the MC, h_b, is of 115 mm (from MC bottom to the top of the blades of the plastic grass). The emergent trees are modelled by wooden rigid cylindrical stems, with a staggered distribution, as shown in Figure 2. The cylinder diameter, D, is of 1 cm, and the stem density N is of 81 stems/m².

2.2 *Flow conditions*

Table 1. Flow conditions of the test cases. Total flow rate Q = 162 L/s. The discharges in the right-hand FP, left-hand FP and MC are denoted Q_r, Q_l, and Q_m, respectively.

Case	Inlet conditions		MC flow depth *
	Q_r+Q_l (L/s)	Q_m (L/s)	h_m (mm)
Uniform Meadow	36	126	171
Uniform Stems	28	134	214
Meadow / Stems	36	126	211-216
Meadow / Stems	52	110	216-216
Stems / Meadow	24	138	170-161
Stems / Meadow	36	126	184-170

* for the roughness transitions, variation between the most upstream and downstream measuring sections

The flow conditions of the test cases are reported in Table 1. The total flow rate, Q = 162 L/s, is constant from one test case to another. Two uniform geometries were investigated: the FP is covered over its entire length (18m) either by (1) plastic grass only, or (2) cylinder arrays installed on the plastic grass. In Table 1, the corresponding flow cases are denoted 'Uniform Meadow' and 'Uniform Stems', respectively.

Two non-uniform geometries were investigated: FP with (1) a transition from plastic grass to cylinder arrays installed on the plastic grass (denoted "Meadow / Stems"), or (2) vice versa ("Stems/Meadow"). The change in roughness is located at mid-length of the flume, where the origin of the x-axis was chosen (x = 0).

In the presence of a roughness transition, preliminary investigations showed that the flow dynamics was dependent on the upstream discharge distribution between the MC and the FP, especially upstream from the step change in roughness (this part is named "upstream reach" in the following). As a result, this inlet boundary condition was modified, to obtain a lateral mean flows between the MC and FP of variable direction and magnitude, which in turn is expected to have a variable impact on the shear-layer turbulence (see Proust et *al.* 2013). The inlet discharges in the MC, Q_m, and in both FP, $Q_l + Q_r$, are reported in Table 1.

2.3 *Flow depth and velocity measurements*

The flow depth was measured with an ultrasonic sensor (UNDK20I69, Baumer) with an accuracy of ± 0.5 mm. A side-looking ADV probe (Vectrino Plus, Nortek) was used to measure the velocity. The convergence of the Reynolds stresses and turbulent intensities was ensured with 18000 samples (acquisition rate = 100 Hz, recording time = 180 s).

Velocity is measured with a lateral step Δy in the range 1 cm to 10 cm (smaller values inside the mixing layer), and with 20 to 25 points for each vertical profile in the MC, or 9 to 13 in the FP. For instance, for the "Uniform Meadow" case, the mesh is composed of 300 points in the MC and of 125 points in each FP.

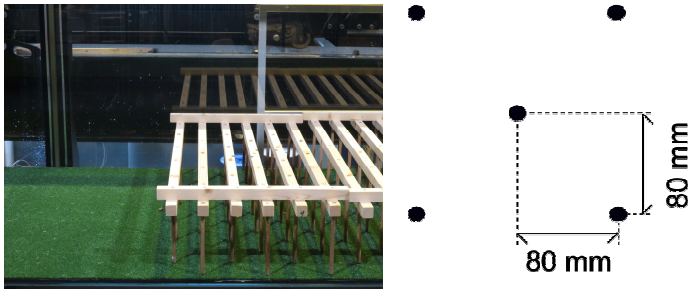

Figure 2. (Left) Close-up side view of the roughness transition. (Right) Sketch of the distribution of wooden rigid cylindrical stems (top view). The cylinder diameter is 10 mm.

For the uniform flows, three longitudinal profiles of flow depth are measured in each sub-section. For the roughness transitions, the flow depth profile is

measured at the centerline position in the MC, *i.e.* at y = 1500 mm. Each flow depth is measured with an acquisition rate of 50 Hz, during 3 minutes.

3 THE INDEPENDENT SUB-SECTIONS METHOD

3.1 *Mass and momentum equations for steady flows*

The ISM consists in a set of three coupled 1D-momentum equations (formulated within the MC, left-hand and right-hand FP) and a mass conservation equation on the total cross-section (see Proust *et al.* 2009).

At the vertical interfaces between MC and FP, the depth-averaged Reynolds-stress, the mass and momentum exchanges by the mean flow are all explicitly accounted for. The 1D momentum equations in the three rectangular sub-sections read

$$\left(1-\frac{U_r{}^2}{gh_r}\right)\frac{dh_r}{dx}=S_o-S_r^f-S_r^D+\frac{\tau_{rm}.h_r}{\rho gA_r}+\frac{q_{rm}\left(2U_r-U_{\text{int}.rm}\right)}{gA_r} \tag{1}$$

$$\left(1-\frac{U_l{}^2}{gh_l}\right)\frac{dh_l}{dx}=S_o-S_l^f-S_l^D+\frac{\tau_{lm}.h_l}{\rho gA_l}+\frac{q_{lm}\left(2U_l-U_{\text{int}.lm}\right)}{gA_l} \tag{2}$$

$$\left(1-\frac{U_m{}^2}{gh_m}\right)\frac{dh_m}{dx}=S_o-S_m^f-\frac{\tau_{lm}.h_l}{\rho gA_m}-\frac{\tau_{rm}.h_r}{\rho gA_m}\ldots \\ \ldots-\frac{q_{lm}\left(2U_m-U_{\text{int}.lm}\right)}{gA_m}-\frac{q_{rm}\left(2U_m-U_{\text{int}.rm}\right)}{gA_m} \tag{3}$$

where U_i = sub-section-averaged velocity; h_i = sub-section flow depth, with i = l, r or m; τ_{ij} = depth-averaged shear stress at the vertical interface between sub-sections i and j; q_{ij} = lateral discharge per unit length between sub-sections i and j; $U_{\text{int}.lm}$ (resp. $U_{\text{int}.rm}$) = longitudinal depth-averaged velocity at the interface MC / left FP (resp. MC / right FP).

In each sub-section, S_i^f is the sub-section friction slope, and S_i^D is the head loss originating from the volume drag force.

It should be noted that in equations 1 to 3, it is implicitly assumed that the water surface is transversally horizontal. This implies that $Z_m = Z_l = Z_r$, if Z_i is the mean water surface level in a sub-section relative to a reference datum.

Lastly, the equation of mass conservation formulated on the total cross-section reads

$$\frac{dQ_m}{dx}+\frac{dQ_l}{dx}+\frac{dQ_r}{dx}=0 \tag{4}$$

3.2 *Bed-friction and drag force*

The friction slope, S_i^f, is computed with the Manning's formula applied to a sub-section

$$S_i^f=\frac{n_i^2U_i^2}{R_i^{4/3}} \tag{5}$$

where R_i is the hydraulic radius accounting for solid walls only, and n_i is the Manning's roughness coefficient. Each sub-section coefficient was calibrated in single channel (FP isolated from the MC with a vertical wall) with a variable flow rate: n_m = 0.0096 in the MC and $n_l = n_r$ = 0.0166 s/m$^{1/3}$ in both FP.

The volume drag force exerted by an array of rigid stems is modelled by a formula established by Nepf (1999). This formula was validated in single open-channel with transitions Meadow/Stems and Stems/Meadow by Dupuis *et al.* (2015). The sub-section head loss S_i^D reads

$$S_i^D=\frac{aC_DU_i^2}{2g} \tag{6}$$

where a = frontal surface per unit volume ($a = ND$ = 0.81 m^{-1}); C_D = drag coefficient related to each stem.

According to Nepf (1999), the drag coefficient is dependent on both the lateral and longitudinal distances between two stems, due to the possible interaction between the cylinder wakes. In the present case (Fig. 2), these distances are such that the interaction is negligible, resulting in a constant drag coefficient C_D = 1.2.

3.3 *Lateral exchanges between sub-sections*

The interfacial depth-averaged Reynolds stress between two sub-sections i and j, τ_{ij}, is modelled by a mixing model in the horizontal plane used by Bousmar & Zech (1999):

$$\left|\tau_{ij}\right|=\rho\Psi^t\left(U_i-U_j\right)^2 \tag{7}$$

where Ψ^t is a constant coefficient of turbulent exchange.

The simulations are carried out using Ψ^t = 0.02, the mean value used in Proust *et al.* (2009), calibrated in three various flumes with smooth FP.

In equations 1 to 3, the head loss caused by the turbulent exchanges between MC and FP reads

$$S_i^t=\pm\sum_j\frac{\tau_{ij}h_i}{\rho gA_i} \tag{8}$$

The interfacial depth-averaged velocity $U_{\text{int}.ij}$ between the sub-sections i and j is modelled as follows

$$U_{\text{int}.ij}=U_i \tag{9}$$

when a lateral mass transfer by the mean flow occurs from sub-section *i* to *j*.

According to Proust *et al.* (2010), the head loss caused by the momentum transfer by the lateral mean flow reads

$$S_i^m = \pm \sum_j \frac{q_{ij}\left(U_i - U_{\text{int}.ij}\right)}{gA_i} \quad (10)$$

This head loss is thus included in the last terms of Equation 1 to 3.

The ISM simultaneously solves the equations 1,2,3 and 4. The quadruplet $\{dh_l/dx; dU_l/dx; dU_m/dx; dU_r/dx\}$ is solved with an explicit method, iteratively, by considering the measured upstream sub-section discharges, $Q_{i,}$ and the measured downstream water level.

4 SIMULATIONS AGAINST MEASUREMENTS

The results presented herein focus on the flow cases with the same inlet conditions, namely Q_r+Q_l (L/s) = 36 L/s (see Table 1), but with opposite roughness transitions: Stems / Meadow and Meadow / Stems.

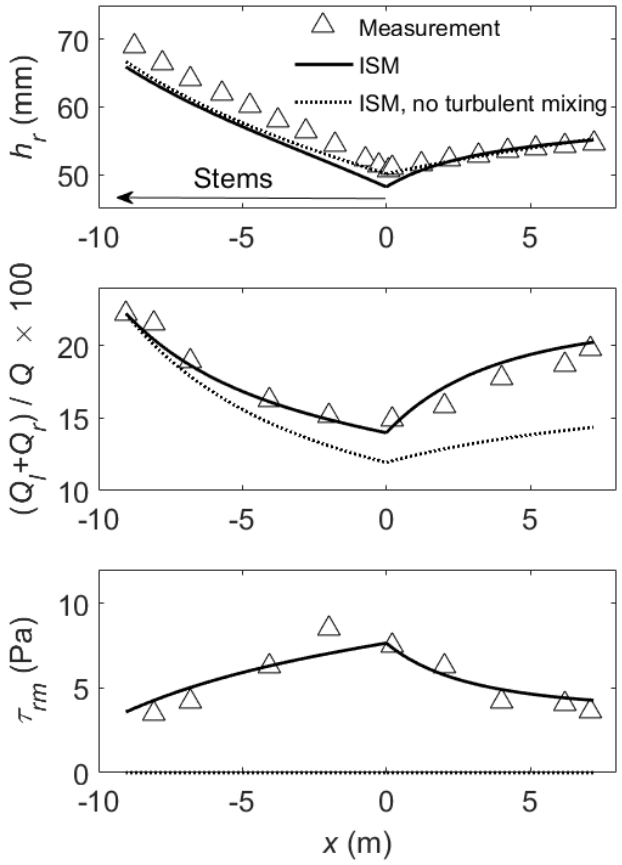

Figure 3. Transition Stems / Meadow with FP inflow Q_r+Q_l = 36 L/s. Streamwise profiles of flow depth in the right-hand FP, h_r, discharge ratio in both FP, $(Q_l+Q_r)/Q$, and interfacial depth-averaged Reynolds-stress between the right-hand FP and the MC, τ_{rm}. Measurements against ISM simulations by considering the horizontal turbulent mixing at the junction MC/FP or neglecting it.

The ISM simulations against experimental data for the two transitions are displayed in Figures 3-4. In both figures are added simulations without accounting for the interfacial turbulent mixing in the horizontal plane (coefficient $\psi^t = 0$ in Eq. 7).

Along the two roughness transitions and irrespective of the direction of the lateral mean flow (decrease or increase in FP flow rate), the simulations of the flow depth in the right-hand FP, h_r, and discharge ratio in both FP, $(Q_l+Q_r)/Q$, are in good agreement with the experimental data. This shows the ability of the coupled system of equations to predict both flow depth and sub-section mean flow with rough FP, with bed-roughness or/and emergent macro-roughness.

The prediction of the interfacial Reynolds-stress can be less accurate, with a maximum relative error of 27 % observed for the Meadow/Stems transition through the stems (Fig. 4). However, the streamwise evolution of this parameter is qualitatively well captured.

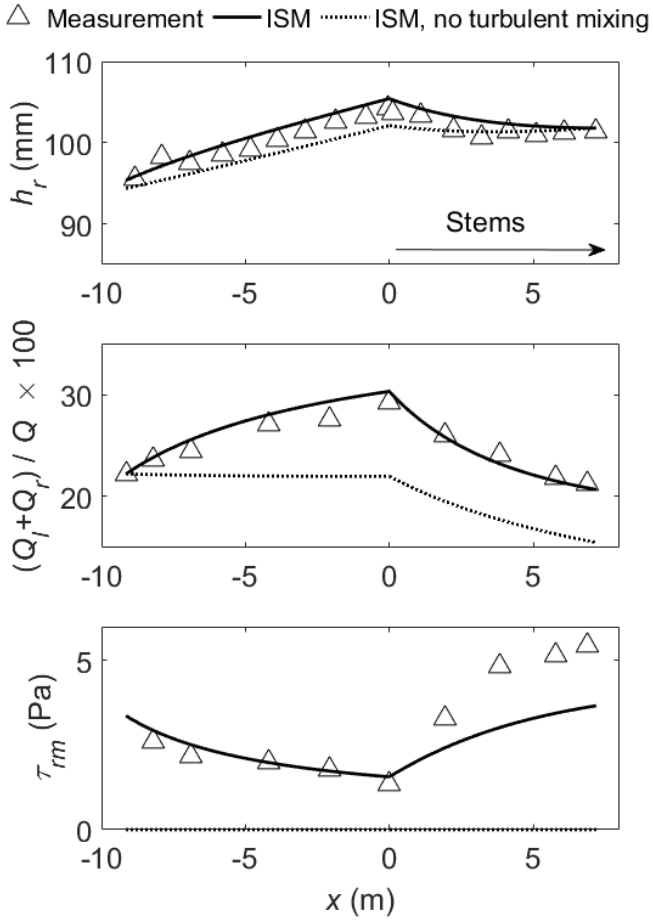

Figure 4. Transition Meadow / Stems, with FP inflow Q_r+Q_l = 36 L/s. Streamwise profiles of flow depth h_r and discharge ratio $(Q_r+Q_l)/Q$ in both FP, and interfacial depth-averaged Reynolds-stress τ_{rm}. Measurements against ISM simulations by considering or neglecting the horizontal turbulent mixing.

To understand these results, and the differences in the simulations when neglecting the horizontal tur-

bulent mixing, Figures 5-6 show the four contributions to energy losses: the head loss related to (1) bed friction, S_i^f; (2) turbulent exchange, S_i^t; (3) the momentum transfer by the lateral mean flow, S_i^m; and (4) the volume drag force, S_i^D.

The most significant contribution to head losses in the FP is the drag force caused by the emergent stems, as shown by the top diagrams in Figures 5-6. This source of head loss primarily drives the water surface profile.

Through the emergent rigid vegetation, the top diagrams in Figures 5-6 also show that the turbulent mixing between MC and FP is also a significant physical process, which drives the discharge distribution between the two sub-sections (see the ratio $(Q_r + Q_l) / Q$ in Figures 3-4). This result is also valid in the meadow reach, both in the MC and the FP.

Lastly, Figures 5-6 show that the head losses by turbulent exchange or by mean flow are of the same order of magnitude, when they are both modelled. As a result, the assumptions that are made in the modelling of the interfacial Reynolds stress (Eq. 7) and of the interfacial streamwise velocity (Eq. 9) are both of primary importance.

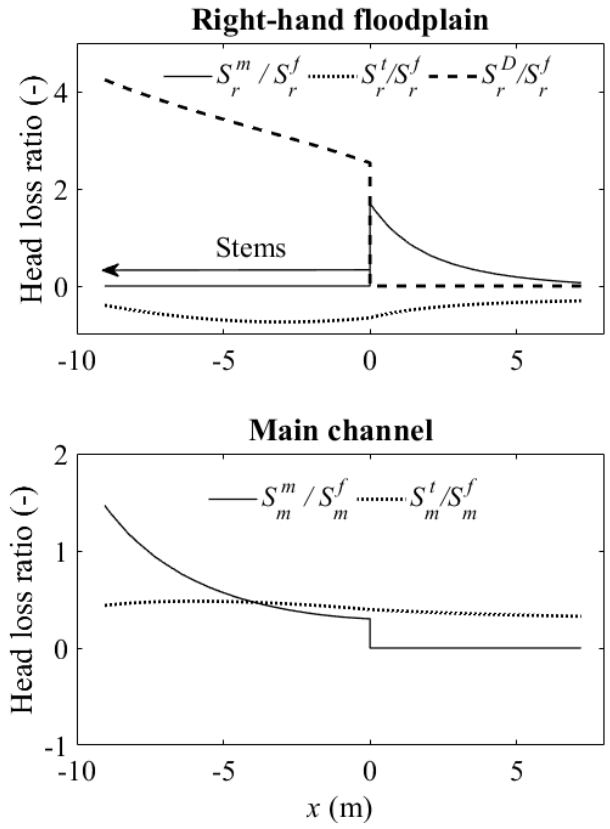

Figure 5. Transition Stems / Meadow, FP inflow Q_r+Q_l = 36 L/s. Head loss related to (1) turbulent mixing S_i^t, (2) momentum transfer by the mean flow, $S^m{}_i$, (3) volume drag force, $S^D{}_i$, compared with bed friction slope S_i^f . Subscript $i = r$ and m in the right-hand FP and MC, respectively.

Regarding the interfacial streamwise velocity, the Equation 9 is a good or rough approximation depending on the flow conditions and on the longitudinal change in the geometry (see Proust *et al.* 2009).

In the present case, this is a rough approximation, as shown in Figure 7 in the case of the transition Meadow / Stems, especially at the far end of the flume. The Equation 9 is physically based, in accordance with the direction of the lateral flow, but it does not take into account the lateral shape of the mixing layer, its lateral location, the presence/absence of 2D horizontal coherent structures (see Proust *et al.* 2016).

As a result, a calibration coefficient φ should be used, such as

$$U_{\text{int}.ij} = \varphi U_i + (1-\varphi) U_j \tag{11}$$

along each homogeneous reach.

In a similar way, the turbulent exchange coefficient Ψ^t = 0.02 that was calibrated with smooth FP, is likely not suitable to these roughened FP, and may be different with emergent macro-roughness elements and bed roughness over the FP. Additionally, other formulas of the literature than Equation 7 are likely to be adequate, and have to be assessed (*e.g.* formulas proposed by Wormleaton & Merett 1990, Moretta & Martin-Vide 2010, Huthof *et al.* 2008).

A critical analysis of the modelling of these interfacial exchanges is being made, based on the six flow cases reported in Table 1. This should help to better define the scope of use of formulas to model the depth-averaged Reynolds-stress and the interfacial velocity.

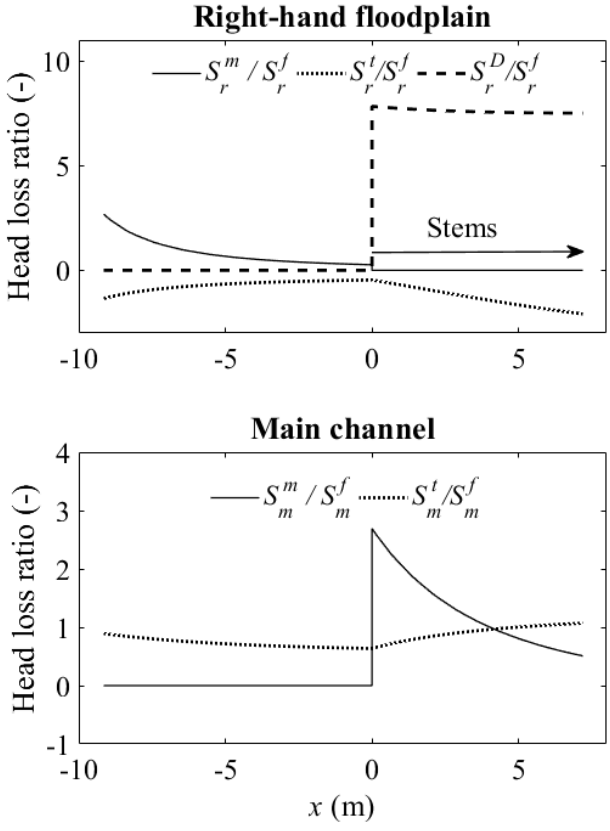

Figure 6. Transition Meadow / Stems, FP inflow Q_r+Q_l = 36 L/s. Head loss related to (1) turbulent mixing S_i^t, (2) momentum transfer by the mean flow, $S^m{}_i$, (3) volume drag force, $S^D{}_i$, compared with bed friction slope S_i^f . Subscript $i = r$ and m in the right-hand FP and MC, respectively.

5 CONCLUSIONS

A 1D+ model that solves three momentum equations and one mass conservation, the Independent Sub-sections Method (Proust *et al.* 2009), is used to simulate steady non-uniform overbank flows originating from a streamwise transition from bed-friction to emergent rigid vegetation drag over the FP (transition Meadow / Stems), or vice versa (transition Stems /Meadow). A volume drag force (Nepf 1999) is included in the momentum equations formulated in the FP. These non-uniform flows were experimentally investigated by Dupuis (2016) in a 18 m long and 3m wide laboratory flume.

The 1D+ model quite accurately predicts the flow depth profile and the discharge distribution between the MC and the FP. Larger errors in the prediction of the interfacial depth-averaged Reynolds stress are observed, especially in the stems region (up to 27%).

Along both roughness transitions, the flow depth profile is mostly controlled by the head loss caused by the emergent stems drag.

In addition to this head loss and to the classical bed-friction, the head losses originating from the horizontal turbulent mixing and the lateral mean flow were found to have an important impact on the discharge distribution between the MC and FP.

The modelling of the interfacial depth-averaged velocity and Reynolds stress is a key point, to accurately predict this discharge distribution. The scope of use of the formulas presented here is being analyzed, according to the presence of bed-roughness versus macro-roughness and to the direction of the lateral flow.

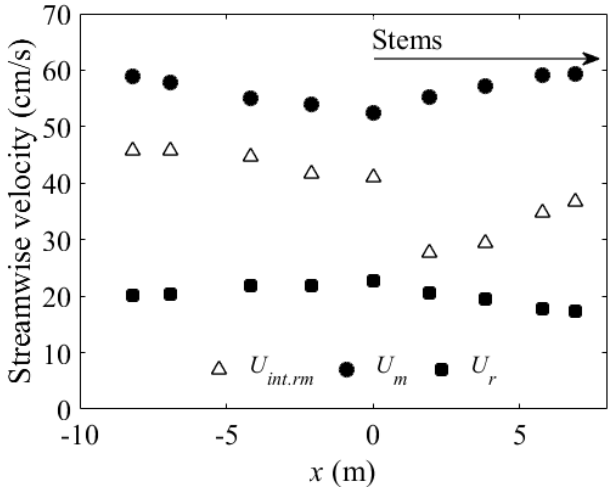

Figure 7. Transition Meadow / Stems, FP inflow Q_r+Q_l = 36 L/s. Measured depth-averaged velocity at the interface right-hand FP / MC, $U_{int.rm}$, and measured average velocities in the MC and right-hand FP, U_m and U_r.

NOTATIONS

Subscripts

i or j = refers to a sub-section (i or j = l, r or m)

l = refers to the left-hand floodplain

m = refers to the main channel

r = refers to the right-hand floodplain

A_i = sub-section area;

B_i = sub-section width;

C_D = drag coefficient for each stem

D = stem diameter

h_b = bank full flow depth in the main channel;

h_i = sub-section flow depth;

n_i = Manning's roughness coefficient;

N = number of stems per surface unit;

q_{ij} = lateral discharge per unit length between sub-sections i and j;

Q = total discharge;

R_i = hydraulic radius;

S_0 = longitudinal bed slope;

S^f_i = sub-section friction slope;

S^t_i = head loss due to horizontal turbulent mixing;

S^D_i = head loss due to the volume drag force caused by the emergent rigid stems;

S^m_i = head loss due to the momentum transfer by the lateral mean flow;

U_i = sub-section mean velocity;

$U_{int.ij}$ = longitudinal depth-averaged velocity at the interface between sub-sections i and j;

Z = water level above reference datum;

τ_{ij} = Reynolds shear stress at the vertical interface between two parallel sub-sections i and j along x-axis (depth-averaged value);

ψ^t = coefficient of turbulent exchange

ACKNOWLEDGEMENT

The authors thank Fabien Thollet for his technical support during the laboratory experiments. The PhD-scholarship of V. Dupuis was half funded by the French National Research Agency (FlowRes project, under grant n°ANR-14-CE03-0010).

REFERENCES

Bousmar D., Zech Y. 1999. Momentum transfer for practical flow computation in compound channels. *Journal of Hydraulic Engineering*. ASCE, 125 (7), 696-706.

Dupuis, V., Proust, S., Berni, C., Paquier, A., Thollet, F. 2015. Open-channel flow over a longitudinal roughness transition from highly-submerged to emergent vegetation. *Proceedings of the 36th IAHR World Congress.* 28 june – 3 July, 2015, The Hague, the Netherlands.

Dupuis, V. 2016. Experimental investigation of longitudinal roughness transitions in single and compound channel flows. *PhD Thesis, Université Claude Bernard Lyon 1, Ecole doctorale MEGA*, in prep.

Jacqmin, T., Wyseur, S. 2011. Influence de la rugosité sur les écoulements en lits croisés dans les rivières à lits composés: Approche numérique et expérimentale. *Mémoire de fin d'étude.* Université catholique de Louvain.150 p.

Huthoff F., Roos P.C., Augustijn D.C.M., Hulscher S.J.M.H. 2008. Interacting Divided Channel Method for Compound

Channel Flow. *Journal of Hydraulic Engineering*. ASCE 134(8), 1158-1164.

Moreta P., Martin-Vide J. 2010. Apparent friction coefficient in straight compound channels. *Journal of Hydraulic Research*. 48(2), 169-177.

Nepf, H. M. (1999). Drag, Turbulence, and diffusion in flow through emergent vegetation. *Water Resources Research*. 35(2), 479-489.

Pasche, E. and G. Rouve. 1985. Overbank flow with vegetatively roughened flood plains. *Journal of the Hydraulics Division*. ASCE, 111(HY9), 1262-1278.

Proust S., Bousmar D., Rivière N., Paquier A., Zech Y. 2009. Nonuniform flow in compound channel: A 1-D method for assessing water level and discharge distribution. *Water Resources Research*. 45, W12411, 1-16.

Proust, S., D. Bousmar, N. Rivière, A. Paquier and Y. Zech. 2010. Energy losses in compound open channels. *Advances in Water Resources.* 33, 1-16.

Proust, S., J. N. Fernandes, Y. Peltier, J. B. Leal, N. Rivière and A. H. Cardoso. 2013. Turbulent non-uniform flows in straight compound open-channels. *Journal of Hydraulic Research.* 51(6), 656-667.

Proust S., Fernandes, J.N., Leal, J.B., Rivière N., Peltier, Y. 2016. Mixing layer and coherent structures in compound channel flow: effects of velocity ratio, shallowness and streamwise non-uniformity. *Water Resources Research*. (in prep.).

Wormleaton, P. R. and D. J. Merrett. 1990. An improved method of the calculation for steady uniform flow in prismatic main channel/flood plain sections. *Journal of Hydraulic Research.* 28(2), 157-174.